

Using Remote Sensing Data-based Hydrological Model Calibrations for Predicting Runoff in Ungauged or Poorly Gauged Catchments

Yongqiang Zhang¹, Qi Huang², Guanghua Qin³, QiuHong Tang⁴, Changming Liu⁴, Jun Xia⁵, Francis Hock Soon Chiew⁶, and David A. Post⁶

¹Institute of Geographic Sciences and Natural Resources Research

²College of Water Resource & Hydropower, Sichuan University

³Sichuan University

⁴Institute of Geographic Sciences and Natural Resources Research, Chinese Academy of Sciences

⁵State key laboratory of Water Resources and Hydropower Engineering Science, Wuhan University

⁶Commonwealth Scientific and Industrial Research Organisation (CSIRO)

November 26, 2022

Abstract

Because remote sensing (RS) data are spatially and temporally explicit and available across the globe, they have the potential to be used for predicting runoff in ungauged or poorly gauged catchments, a challenging area of research in hydrology over the last several decades. There is potential to use remotely sensed data for calibrating hydrological models in regions with limited streamflow gauges. This study conducts a comprehensive investigation on how to incorporate gridded remotely sensed-evapotranspiration (AET) and water storage data for constraining hydrological model calibration in order to predict daily and monthly runoff in 30 catchments of Yalong River basin, China. To this end, seven RS data calibration schemes are explored, compared to traditional calibration against observed runoff and traditional regionalization using spatial proximity. Our results show that using bias-corrected remotely sensed AET (bias-corrected PML-AET data) for constraining model calibration performs much better than using the non bias-corrected remotely sensed AET data (non bias-corrected AET obtained from PML model estimate). Using the bias-corrected PML-AET data in a gridded way is much better than that in a lumped way, and outperforms the traditional regionalization approach especially at upstream and large catchments. Combining the bias-corrected PML-AET and GRACE water storage data performs similarly to using the bias-corrected PML-AET data only. This study demonstrates that there is great potential to use RS-AET based data for calibrating hydrological models in order to predict runoff in data sparse regions with complex terrain conditions.

1 **Using Remote Sensing Data-based Hydrological** 2 **Model Calibrations for Predicting Runoff in** 3 **Ungauged or Poorly Gauged Catchments**

4 Qi Huang^{1,2,6}, Guanhua Qin^{1,3,6}, Yongqiang Zhang^{2*}, QiuHong Tang², Changming
5 Liu², Jun Xia⁴, Francis H.S. Chiew⁵, and David Post⁵

6 ¹College of Water Resource & Hydropower, Sichuan University, Chengdu 610065,
7 China;

8 ²Key Laboratory of Water Cycle and Related Land Surface Processes, Institute of
9 Geographic Sciences and Natural Resources Research, Chinese Academy of Sciences,
10 Beijing 100101, China

11 ³State Key Laboratory of Hydraulics and Mountain River Engineering, Sichuan
12 University, Chengdu 610065, China

13 ⁴State Key Laboratory of Water Resources & Hydropower Engineering Sciences ,
14 Wuhan University, 430072, Wuhan, China

15 ⁵CSIRO Land and Water, Black Mountain, Canberra, ACT 2601, Australia

16 ⁶These authors contributed equally to this work.

17 *Corresponding author: Yongqiang Zhang

18 (yongqiang.zhang2014@gmail.com; zhangyq@igsnr.ac.cn)

19 **Key points**

- 20 • Using remote sensing data to calibrate hydrological model shows great potential
- 21 especially at upstream and large areas in Yalong River basin

- 22 • Compared to raw PML-AET, bias-correction of PML-AET improves runoff
- 23 prediction noticeably and adding GRACE shows limited benefit

- 24 • Gridded modelling calibrated at each grid performs noticeably better than lumped
- 25 modelling calibrated at each catchment

26 **Abstract**

27 Because remote sensing (RS) data are spatially and temporally explicit and available
28 across the globe, they have the potential to be used for predicting runoff in ungauged
29 or poorly gauged catchments, a challenging area of research in hydrology over the last
30 several decades. There is potential to use remotely sensed data for calibrating
31 hydrological models in regions with limited streamflow gauges. This study conducts a
32 comprehensive investigation on how to incorporate gridded remotely
33 sensed-evapotranspiration (AET) and water storage data for constraining hydrological
34 model calibration in order to predict daily and monthly runoff in 30 catchments of
35 Yalong River basin, China. To this end, seven RS data calibration schemes are
36 explored, compared to traditional calibration against observed runoff and traditional
37 regionalization using spatial proximity. Our results show that using bias-corrected
38 remotely sensed AET (bias-corrected PML-AET data) for constraining model
39 calibration performs much better than using the non bias-corrected remotely sensed
40 AET data (non bias-corrected AET obtained from PML model estimate). Using the
41 bias-corrected PML-AET data in a gridded way is much better than that in a lumped
42 way, and outperforms the traditional regionalization approach especially at upstream
43 and large catchments. Combining the bias-corrected PML-AET and GRACE water
44 storage data performs similarly to using the bias-corrected PML-AET data only. This
45 study demonstrates that and there is great potential to use RS-AET based data for

46 calibrating hydrological models in order to predict runoff in data sparse regions with
47 complex terrain conditions.

48 **Key words:** Remote sensing, evapotranspiration, PML, runoff prediction, grid, bias
49 correction

50 **1. Introduction**

51 Runoff Prediction in Ungauged Basins (PUB) is materially important for accounting
52 and managing water resources, and flood disaster risk management (Montanari et al.,
53 2013). A widely used approach for PUB is regionalization that transfers calibrated
54 model parameters from a gauged catchment (or a donor) to an ungauged catchment
55 (Post and Jakeman, 1999; Hundecha and Bardossy, 2004; Merz and Blöschl, 2004;
56 Yadav et al., 2007; Oudin et al., 2008; Zhang and Chiew, 2009; Hrachowitz et al.,
57 2013; Pechlivanidis and Arheimer, 2015; Li and Zhang, 2017). However, the
58 performance of the regionalization approach becomes gradually poorer with an
59 increasing regionalization distance (Li and Zhang, 2017), suggesting that
60 regionalization is highly uncertain in regions with very limited or sparsely distributed
61 streamflow gauges. The data scarcity, and hence the regionalization challenge, is
62 prominent especially in alpine and complex-terrain regions.

63 Remote sensing observation provides continuous data in both spatial and temporal
64 scales, which makes it possible to estimate regional surface meteorological data in a
65 quick, accurate and widely applicable way. Therefore, remote sensing data has been

66 widely applied and combined with hydrological models in ungauged catchments. As
67 inputs to hydrological model, the remote sensing data should be relatively accurate,
68 otherwise it needs to be bias corrected (Stisen and Sandholt, 2010; Habib et al., 2014;
69 Zhang and Tang, 2015). What's more, it has also been shown that constraining
70 multiple variables such as soil moisture and water storage data from remote sensing
71 can improve the performance of hydrological models (Sutanudjaja et al., 2014;
72 Wanders et al., 2014; Li et al., 2016; Kundu et al., 2017; Yassin et al., 2017; Pomeon
73 et al., 2018). Nevertheless, practically all studies calibrate the models against
74 observed streamflow data, which is limited in poorly gauged regions. Zhang et al.
75 (2020) proposed a remotely sensed actual evapotranspiration (RS-AET) calibration
76 approach based on PML evapotranspiration products (PML-AET), and showed that
77 this approach is potentially useful in the relatively wet regions of Australia.
78 Nevertheless, there are several limitations in the study that can be improved upon. First,
79 Zhang et al. (2020) did not consider the potential for improving the quality of the
80 remote sensing actual evapotranspiration data that was used for hydrological model
81 calibration. Second, the study used a lumped catchment-average rainfall-runoff
82 modelling approach and does not take advantage of the spatial continuity of remote
83 sensing data. Third, the research does not consider the potential to combine remote
84 sensing actual evapotranspiration with remote sensing water storage data.
85 To further advance the study of Zhang et al. (2020), this paper proposes a more

comprehensive framework that uses runoff-free or very limited runoff data for hydrological model calibrations. Specifically, this work aims to improve calibration schemes by adding more remote sensing information (non bias-corrected PML-AET, bias-corrected PML-AET, GRACE water storage) into model calibrations, and calibrating the hydrological model both in lumped and gridded ways. Nine modelling schemes (seven are based on RS-data calibrations; one is based on runoff-data calibration; one is based on spatial proximity regionalization) are tested on the Yalong River Basin, the upper reach of which is located on the southeastern Tibetan Plateau and the northwest of Yunnan-Guizhou Plateau, with complex terrain conditions. The major objectives of this study are to:

- i. Evaluate the merit of using limited runoff data for bias correcting remote sensing evapotranspiration data
- ii. Investigate the performance of calibrations with different remote sensing data (non bias-corrected PML-AET, bias-corrected PML-AET, GRACE water storage);
- iii. Evaluate the performance of calibrations at different spatial scales (gridded and lumped); and
- iv. Investigate the spatial characteristics of optimum model calibration schemes.

103 2. Study area and data

104 2.1. Study area

105 The study area is located in the Yalong River basin. The Yalong River, the largest
106 tributary on the left bank of the Jinsha River, originates from the southern foot of the
107 Bayankala Mountains in Yushu County, Qinghai Province. The river flows from the
108 northwest to the southeast, and the length of the mainstream is around 1570 km. The
109 whole basin area is around $1.36 \times 10^5 \text{ km}^2$, shaped like a north-south stripe
110 ($96^\circ 52'E$ - $102^\circ 48'E$, $26^\circ 32'N$ - $33^\circ 58'N$) and located on the southeastern Tibetan Plateau
111 and the northwest of Yunnan-Guizhou Plateau. The river basin spans more than seven
112 degrees of latitude from north to south, and the geographic characteristics in the basin
113 are complex. The altitude varies greatly from 5,400 m to 980 m from the north to the
114 south, with a reduction of 4,420 m, and the terrain mainly includes hilly plateaus,
115 alpine canyons, and wide valley basins from north to south, respectively. All of these
116 make the climate and geography of the basin greatly different in both horizontal and
117 vertical directions.

118 This study uses data from 30 catchments within the Yalong River basin. Fig.1 shows
119 the geographical map of the study area and the information of the 30 catchments. It
120 also summarizes the flow path through the 30 catchments.

121 **Figure 1 is about here**

122 **2.2. Data**

123 The Climate Meteorological Forcing Dataset (simplified as CMFD) is used to drive
124 the hydrological model. The CMFD is a reanalysis product of near-surface
125 meteorological and environmental elements in China. The gridded precipitation data
126 used here is the CMFD-Precipitation. The CMFD-P has been shown to be a high data
127 quality dataset (Yang et al., 2017; Ren et al., 2018; Wu et al., 2019; He et al., 2020),
128 and is also further evaluated here against daily gauged precipitation in the study area
129 (see sections 3.1.1 and 4.1).

130 The gridded actual evapotranspiration data used in this paper is obtained from
131 PML_V2 global evapotranspiration (simplified as PML-AET) product (Zhang et al.,
132 2019). It is referred as ‘non bias-corrected PML-AET’ thereafter. Since this is a global
133 product, it is necessary for bias correction to be applied in order to improve its
134 usability for hydrological modelling applications (see Sections 3.1.2 and 4.2).

135 The water storage data applied in this paper is Gravity Recovery and Climate
136 Experiment’s total water storage anomaly data (simplified as GRACE) and has been
137 corrected by officially provided scale factors (Swenson and Wahr, 2006; Landerer and
138 Swenson, 2012). All the gridded datasets were resampled to 0.05° to match the PML
139 resolution. The daily runoff data is obtained from hydrological observed records, and
140 used here as the reference data for model validation. Table 1 gives more information
141 on those data.

Table 1. Detailed information for research data used in this study

Short name	Detailed Name	Spatial Resolution	Temporal Resolution	Temporal Coverage	Data source	Key references
CMFD	Climate Meteorological Forcing Dataset	0.1°	3-hour	1979-2018	http://westdc.westgis.ac.cn/data/ 7a35329c-c53f-4267-aa07-e0037d913a21	(He and Yang, 2011; Fan et al., 2017; He et al., 2020)
PML_V2	PML_V2 global evapotranspiration and gross primary production	0.05°	8-day	2002.07-2019.08	http://www.tpdac.ac.cn/zh-hans/data/ 48c16a8d-d307-4973-abab-972e9449627c	(Zhang et al., 2019)
GRACE_ RL05	Gravity Recovery and Climate Experiment	1°	1-month	2002.04-2017.02	https://grace.jpl.nasa.gov/data/ get-data/monthly-mass-grids-land/	(Swenson and Wahr, 2006; Landerer and Swenson, 2012)
Meteorological gauge Data	Daily dataset of China's surface climate data	-	1-day	1951-2019	http://data.cma.cn/data/cdcdetail/dataCode/ SURF_CLI_CHN_MUL_DAY_V3.0.html	-
Hydrological station Data	Daily mean runoff of hydrological stations in Yalong River	-	1-day	2004-2012 (Varying across stations)	The information and data of stations are provided by Yalong River hydropower- development company	

143 It should be noted that there are two downstream catchments (Xiaodeshi catchment
144 and Tongzilin catchment) impacted by the Ertan reservoir regulation during
145 2004-2012. To obtain the ‘natural flow’ for these catchments, streamflow series is
146 restored through reservoir dispatching data based on water balance method. As shown

in Fig.1, the Xiaodeshi hydrology station and the Tongzilin hydrology station are in the downstream of the Ertan hydropower station and are both in the mainstream of Yalong River. Ignoring other human activities along the river, the ‘natural flow’ series of Xiaodeshi and Tongzilin catchment is obtained by adding the value of the Ertan Hydropower Station inflow minus the outflow.

3. Methodology

3.1. Data Processing

3.1.1. Evaluation of CMFD-P

As shown in Figure 1, the available rain gauges are few and sparsely distributed. Thus, a set of accurate gridded precipitation dataset is needed. The accuracy of CMFD-P data is evaluated against ten surface meteorological precipitation gauges in the Yalong River Basin. The main idea is to verify the accuracy through detect ability and accuracy indicators. The evaluation indicators are listed in Table 2, together with their descriptions.

Table 2. Evaluation indicators for precipitation

Type of Indicators	Evaluation Indicators	Short name	Formula	Ideal Value
Detect Ability Indicators	Probability Of Detection	<i>POD</i>	$POD = \frac{n_{11}}{n_{11} + n_{01}}$	1
	Frequency Of Hit	<i>FOH</i>	$FOH = \frac{n_{11}}{n_{11} + n_{10}}$	1

Accuracy Indicators	Heidke's Skill Score	<i>HSS</i>	$HSS = \frac{2(n_{11}n_{00} - n_{10}n_{01})}{(n_{11} + n_{01})(n_{01} + n_{00}) + (n_{11} + n_{10})(n_{10} + n_{00})}$	1
	Correlation coefficient	<i>CC</i>	$CC = \frac{\sum_{i=1}^n (P_i - \bar{P})(G_i - \bar{G})}{\sqrt{\sum_{i=1}^n (P_i - \bar{P})^2 \sum_{i=1}^n (G_i - \bar{G})^2}}$	1
	Nash-Sutcliffe Efficiency	<i>NSE</i>	$NSE = 1 - \frac{\sum_{i=1}^n (P_i - G_i)^2}{\sum_{i=1}^n (G_i - \bar{G})^2}$	1
	Similarity indicator	<i>SI</i>	$SI = 1 - \frac{\sum_{i=1}^n (P_i - G_i)^2}{\sum_{i=1}^n (G_i - \bar{G} + P_i - \bar{G})^2}$	1
	Mean error	<i>ME/(mm)</i>	$ME = \sum_{i=1}^n (G_i - P_i) / n$	0
	Mean absolute error	<i>MAE/(mm)</i>	$MAE = \sum_{i=1}^n G_i - P_i / n$	0
	Bias	<i>BIAS</i>	$BIAS = \sum_{i=1}^n (G_i - P_i) / \sum_{i=1}^n G_i$	0
	Absolute bias	<i>ABIAS</i>	$ABIAS = \sum_{i=1}^n G_i - P_i / \sum_{i=1}^n G_i$	0

* n_{11} represents the frequency of precipitation detected by both CMFD and the rainfall gauges; n_{10} represents the frequency of precipitation detected by CMFD but not the rainfall gauges; n_{01} represents the frequency of precipitation detected by the gauges but not CMFD; n_{00} represents the frequency of precipitation detected by neither CMFD nor the rainfall gauges. P represents precipitation in CMFD, G represents gauged precipitation, and n is the amount of samples.

3.1.2. Bias correction of PML-AET

The PML-V2 is a global evapotranspiration and gross primary product. It therefore needs to be bias corrected for application at small spatial scales and local regions. In addition, the actual evapotranspiration can be directly validated and bias corrected

170 using the water balance method. The mean annual PML-AET is bias corrected here to
 171 match the mean annual precipitation minus mean annual runoff estimated by the Fu
 172 model (the Fu model is an adaption of the Budyko framework) (Fu, 1981; Zhang et al.,
 173 2004; Zhang et al., 2008). The bias correction is carried out as follows:

174 i. In order to use minimum possible observed runoff data for the bias correction and to
 175 maximize the usability of the PML-AET model calibrations, mean annual observed
 176 runoff data (Q_{obs}) of a downstream basin, Daluo (Gauging station 21, see Fig.1) for the
 177 period of 1999 to 2012 is used for the method inputs (this was the length of streamflow
 178 data available at Daluo). What's more, mean annual gridded precipitation data
 179 (CMFD-P) and mean annual gridded potential evaporation E_p are also used for the
 180 method inputs. E_p is estimated using the Allen et al. (2006) equation following
 181 Penman-Monteith method (*Eq. 1*). The input data comes from the CMFD dataset (i.e.
 182 temperature, humidity, wind speed), digital elevation model (latitude and longitude),
 183 and daily dataset of China's surface sunshine duration data that was spatially
 184 interpolated by kriging method (Delhomme, 1978)). E_p is calculated using the
 185 following equation:

$$186 \quad E_p = \frac{0.408\Delta(R_n - G) + \gamma \frac{900}{T_{mean} + 273} u_2 (e_s - e_a)}{\Delta + \gamma(1 + 0.34u_2)}, \quad (1)$$

187 where E_p is the potential evaporation (mm/d); Δ is the slope of the saturation vapor
 188 pressure versus temperature curve (kPa/°C); R_n is the net radiation flux density at the

189 surface (MJ/(m*d)); G is the sensible heat flux from the surface to the soil (MJ/(m²*d));
 190 γ is the psychometrics constant (kPa/°C); T_{mean} is the daily temperature (°C); u_2 is the
 191 wind speed at 2-m height (m/s); e_s is the saturation vapor pressure at air temperature
 192 (kPa); e_a is the actual vapor pressure of the air (kPa).

193 ii. A single value of the parameter α in the Fu model is 1.56, estimated based on the
 194 basin-average mean annual precipitation and potential evaporation at Daluo
 195 catchment from 1999 to 2012. This α value of 1.56 is used to calculate Q_{fu} at each
 196 (0.05° x 0.05°) of 5170 grid cells within the study area for the period of 2004 to 2012.
 197 Q_{fu} is expressed as:

$$198 \quad Q_{fu} = P[1 + (AI)^{\delta}]^{1/\delta} - E_p, \quad (2)$$

199 where Q_{fu} represents mean annual runoff (mm/year). P is mean annual rainfall
 200 (mm/year). E_p is mean annual potential evapotranspiration (mm/year). AI is the aridity
 201 index, calculated as E_p divided by P .

202 iii. The ‘real’ value of mean annual AET (2004-2012) at each grid is calculated as P
 203 minus Q_{fu} ;

204 iv. A scaling factor SC at each grid cell is calculated as the ‘real’ mean annual AET
 205 divided by mean annual Non bias-corrected PML-AET; and

206 v. Finally, the bias-corrected PML-AET for each grid is obtained by multiplying the
 207 non bias-corrected PML-AET by the scaling factor at each grid.

208 In summary, this study uses mean annual streamflow data from one downstream
209 gauge of Daluo and from an independent period of 1999-2012 to parameterize the Fu
210 model, and then uses Fu mean annual runoff estimate to bias correct PML-AET at each
211 grid cell in 2004-2012.

212 **3.2. Xinanjiang Model**

213 The Xinanjiang model is a lumped conceptual model, was developed by Zhao (1980).
214 The model has been extensively used for runoff simulation and prediction across humid
215 and semi-humid regions globally (Zhao, 1992; Jayawardena and Zhou, 2000; Cheng et
216 al., 2006; Ju et al., 2009; Li et al., 2009; Yao et al., 2009). The model is driven by daily
217 precipitation and potential evapotranspiration for the period of 2004-2012. The model
218 outputs include daily runoff and daily actual evapotranspiration. Daily water storage is
219 one of state variables in this model and is used in the calibration functions in this study.
220 The model structure is shown in Figure 2.

221 **Figure 2 is about here**

222 **3.3. Model calibration schemes**

223 The RS-ET runoff free calibration method is developed by Zhang et al. (2020) and its
224 objective function is calibrated only against PML-AET. It has been shown that water
225 storage data can also enhance hydrological model calibration (Yassin et al., 2017).
226 This study will therefore explore the model calibration against both remotely sensed

227 (and bias corrected) PML-AET and water storage data. This study also assesses the
228 model calibrations at three spatial scales: grid, region and catchment. This means that
229 the model is calibrated at each grid, region, and catchment, respectively. As a result,
230 for grid calibration, each grid cell has one calibration parameter set; for region
231 calibration, each grid has one calibration parameter set; for catchment calibration,
232 each catchment has one calibration parameter set. The model becomes more lumped
233 with the scale increase from grid to catchment.

234 Altogether, nine calibration schemes are considered (Table 3), seven of which are
235 based on PML-AET calibration methods and two of which are based on streamflow
236 calibration. A global optimizer, the genetic algorithm built in MATLAB (Holland,
237 1992; Konak et al., 2006), is used to optimize model parameters. Scheme 1 is
238 calibrated against observed daily runoff by using lumped catchment inputs, which
239 represents the best simulation capability in each catchment. Scheme 2 is regionalization
240 based on spatial proximity (i.e. selecting a donor catchment with minimum Euclidian
241 distance between centroids of the ‘ ungauged ’ catchment and the donor) (Merz and
242 Blöschl, 2004; Oudin et al., 2008; Li and Zhang, 2017). This scheme is the traditional
243 regionalization approach, regarded as the baseline for evaluating the performance of
244 schemes 3-9. Scheme 3 uses the non bias-corrected PML-AET output for model
245 calibration. Schemes 4-6 apply the bias-corrected PML-AET for model calibration, but
246 the difference among them is scheme 4 for calibration at each PML-AET grid cell,

247 scheme 5 for calibration at each region (The region is defined as the contribution area
 248 between two gauges. Therefore, the lowest-level tributary comprises 1 region, but
 249 higher lever catchments comprise multiple regions. For instance, Ganzi (1), Xinlong (2)
 250 and Gongke (3) have one, two, three regions, respectively), and scheme 6 for
 251 calibration at each catchment. Schemes 7-9 are similar to schemes 4-6, respectively, but
 252 with the model calibrated against both the bias-corrected PML-AET data and the
 253 GRACE water storage data for model calibration.

254 Table 3 summarizes the nine schemes for model calibration and provides the objective
 255 function used for calibration in each scheme.

256 **Table 3.** Summary of nine model calibration schemes 1-9.

257 The numbers 1-9 represent scheme numbers, respectively. Eq. (3)- Eq. (6) represent objective functions.

Calibration Method	At grids	At regions	At catchment	Model input data (and calibration data)	Objective functions
Calibration with observed runoff			1	CMFD-P, Ep, (Q at 30 stations)	Eq.(3)
Regionalization			2	CMFD-P, Ep, a set of parameters (at a neighbor station)	Eq. (3)
Non bias-corrected PML-AET runoff-free calibration approach	3			CMFD-P, Ep, (non bias-corrected PML-AET)	Eq. (4)
Bias corrected PML-AET calibration approach	4	5	6	CMFD-P, Ep, (bias-corrected PML-AET)	Eq. (5)
Bias corrected PML-AET combined with GRACE storage data runoff-free calibration approach	7	8	9	CMFD-P, Ep, (bias-corrected PML-AET, GRACE)	Eq. (6)

258 The widely used Nash-Sutcliffe Efficiency (NSE) (Nash and Sutcliffe, 1970) is used as
 259 the objective functions defined in Equations 3-6.

$$260 \quad F_1 = 1 - NSE_Q, NSE_Q = 1 - \frac{\sum_{i=1}^N (Q_{obs} - Q_{sim})^2}{\sum_{i=1}^N (Q_{obs} - \overline{Q_{obs}})^2}, \quad (3)$$

$$261 \quad F_2 = 1 - NSE_{ET1}, NSE_{ET1} = 1 - \frac{\sum_{i=1}^N (AET_{PML} - AET_{SIM})^2}{\sum_{i=1}^N (AET_{PML} - \overline{AET_{PML}})^2}, \quad (4)$$

$$262 \quad F_2 = 1 - NSE_{ET2}, NSE_{ET2} = 1 - \frac{\sum_{i=1}^N (AET_{B-PML} - AET_{SIM})^2}{\sum_{i=1}^N (AET_{B-PML} - \overline{AET_{B-PML}})^2}, \quad (5)$$

$$263 \quad F_3 = (1 - NSE_{ET2}) + (1 - NSE_{\Delta W}), NSE_{\Delta W} = 1 - \frac{\sum_{i=1}^N (\Delta W_{GRACE} - \Delta W_{SIM})^2}{\sum_{i=1}^N (\Delta W_{GRACE} - \overline{\Delta W_{GRACE}})^2}, \quad (6)$$

264 where Q_{obs} represents the observed daily runoff, Q_{sim} represents the simulated daily
 265 runoff. AET_{SIM} , AET_{PML} and AET_{B-PML} represent modeled actual evapotranspiration,
 266 the raw PML-AET output and bias-corrected PML-AET with a temporal step of eight
 267 days, respectively. ΔW_{GRACE} and ΔW_{SIM} with a temporal step of one month represent
 268 the water storage change estimated by GRACE and calculated by Xinanjiang model,
 269 respectively. It is noted that Q_{sim} generated from grid and regional calibrations, is
 270 aggregated to catchment scale to compare to Q_{obs} . The smaller the value of objective
 271 function is, the better the simulation quality.

272 **3.4. Evaluating the nine modelling schemes**

273 The NSE_Q and Qualified Rate (QR) (Standardization Administration of the People's
 274 Republic of China, 2008) is used to evaluate the performance of the nine schemes at

different temporal scales. The model performance is mainly decided by NSE_Q and QR is considered as an assistant indicator. The QR is defined as:

$$QR = \frac{m}{n} \quad (7)$$

where m represents the numbers of samples whose ABIAS are less than 0.35, n is the total number of samples (total number of daily, or monthly streamflow data). The value of NSE_Q varies from negative infinity to 1, the closer to 1 indicating better model performance. The value of QR varies from 0 to 1, the closer to 1 indicating better model performance (QR=1 means that the bias from all samples is less than 0.35). The temporal step is one day and one month for daily runoff and monthly runoff, respectively. The model evaluation period is the period of available observed runoff series in each catchment.

4. Results

4.1. Evaluation of CMFD-P

Figure 3 evaluates CMFD-P, the $0.05^\circ \times 0.05^\circ$ reanalysis precipitation product of China, against ten precipitation gauges at different time scales. Table 4 shows the performance of the CMFD-P using statistical indices summarized from the ten gauges. At daily scale, the values of POD, FOH, and HSS are 0.93, 0.67, and 0.62, respectively. This indicates that the detect ability of CMFD-P is relatively good. The CMFD-P is able to detect most of the daily precipitation events between 2004 and 2012. The accuracy of CMFD-P is

also relatively good at the daily scale with high SI (0.75) and low BIAS (-0.002). On the other hand, the low frequency of hits leads to low NSE (0.26) and high ABIAS (0.83). At the monthly scale, the consistency between the CMFD-P and the station's precipitation has increased significantly compared to the daily scale. The value of accuracy indicators has increased significantly. CC, NSE and SI has increased to 0.99, 0.99 and 1.00, respectively, and ABIAS has decreased dramatically to 0.06. Compared to monthly performance, the performance of CMFD-P at annual scale is slightly degraded, indicated by smaller NSE and SI, but ABIAS at annual scale is 0.02, noticeably smaller than that at monthly scale. In summary, CMFD-P has overall quite good quality in this region. Furthermore, it performs best at monthly scale, followed by annual and daily scales. The poor performance of daily precipitation might bring more uncertainties to the hydrological models, but the high *SI* and low *BIAS* might show positive influence in the modelling.

Figure 3 is about here

Table 4. Evaluation of CMFD-P (precipitation in CMFD). The definition of each index is given in Table 2

	POD	FOH	HSS	ME/mm	BIAS	MAE/mm	ABIAS	CC	NSE	SI
Daily	0.93	0.67	0.62	-0.001	-0.002	1.61	0.83	0.59	0.26	0.75
Monthly	-	-	-	-0.153	-0.002	3.22	0.06	0.99	0.99	1.00
Annual	-	-	-	-0.366	-0.002	13.40	0.02	0.99	0.98	0.99

309 4.2. Bias-corrected PML-AET

310 The non bias-corrected PML-AET and bias-corrected PML-AET are evaluated using
311 their performance for estimating annual streamflow. The annual streamflow of them is
312 estimated by annual precipitation minus annual non bias-corrected PML-AET (Q_1)
313 and annual precipitation minus annual bias corrected PML-AET (Q_2), respectively. If
314 the consistency between Q_2 and Q_{obs} is much better than it between Q_1 and Q_{obs} , the bias
315 correction improves the accuracy of the AET estimation.

316 Figure 4 summarizes the performance of Q_1 and Q_2 at annual scale for all 30 streamflow
317 gauges. It is clear that Q_2 is noticeably better than Q_1 . In most basins, scatters of Q_{obs}
318 against Q_2 distribute evenly on both sides of the 1: 1 line, which means the consistency
319 between Q_2 and Q_{obs} is good, while Q_1 is severely biased. This result demonstrates that
320 the bias-corrected PML-AET achieves much better water balance (in terms of
321 producing streamflow), compared to the non bias-corrected PML-AET. It should be
322 noted that the Q_{obs} at Daluo station was used to bias correct PML-AET. Therefore, the
323 performance of bias correction of mainstream catchments in the upper reach of Daluo
324 catchment (Daluo, Luning, Jinping, Maidilong, Jiju and Yajiang) is better than that in
325 other catchments. The better bias correction might improve the performance of
326 hydrological model in these catchments.

327 **Figure 4 is about here**

328 4.3. Runoff prediction

329 Figure 5 summarizes the performance of nine modelling schemes in predicting daily
330 runoff (5a,5c) and monthly runoff (5b,5d) across 30 catchments in the Yalong River
331 basin (to present patterns clearly, several negative values are not shown here, but are
332 shown latter in Fig.6). In each scheme, the simulated monthly runoff is accumulated
333 by daily runoff and generally performs better than daily runoff with a higher mean
334 value. The annual runoff performance has not been analyzed because of short records
335 of yearly observed runoff. NSE describes modeling ability, QR describes the modeling
336 quality. The range of NSE and QR describes modeling stability and the model performs
337 better with a lower range of NSE and QR.

338 **Figure 5 is about here**

339 4.3.1. Non bias-corrected PML-AET calibration versus bias-corrected PML-AET 340 calibration

341 The simulated streamflow obtained from scheme 3 (calibration using the non
342 bias-corrected PML-AET data) and from scheme 4 (calibration using the
343 bias-corrected PML-AET data) are evaluated against observed streamflow at daily
344 and monthly scales. Scheme 3 gives a result of mean NSE of -0.08 and mean QR of
345 0.15 for daily runoff simulation, while mean NSE of -0.01 and mean QR of 0.15 for
346 monthly runoff simulation, indicating very poor accuracy in the modelling. For daily
347 runoff in scheme 4, the mean NSE is 0.39 and the mean QR is 0.40, while for monthly

runoff in scheme 4, the mean NSE is 0.65 and the mean QR is 0.45. Compared to scheme 3, the performance of scheme 4 is greatly improved noticeably with increment of 0.47 in mean NSE and 0.25 in mean QR for daily runoff, and an increment of 0.66 in mean NSE and 0.30 in mean QR for monthly runoff. Therefore, using the bias-corrected PML-AET data for constraining model calibration performs much better than using the non bias-corrected PML-AET data, and the improvement in monthly runoff simulation is larger than that in daily runoff simulation. Therefore, in the following sections of 4.3.2-4.3.4, we only show the relative merits related to bias-corrected PML-AET (i.e. schemes 4-9).

4.3.2. Lumped calibration versus gridded calibration

The bias-corrected PML-AET data, as well as its combination with the GRACE data are used to calibrate model parameters in Schemes 4-6 and Schemes 7-9, respectively. The difference in Schemes 4-6 is the spatial scale becomes more lumped with the increase of the scheme number and scheme 7-9 repeat the spatial scale of schemes 4-6. For daily runoff simulation, the mean NSE of schemes 4-9 is 0.39, 0.32, 0.26, 0.39, 0.31 and 0.27, respectively; the mean QR of schemes 4-9 is 0.40, 0.37, 0.29, 0.40, 0.40 and 0.29, respectively. For monthly runoff simulation, the mean NSE of schemes 4-9 is 0.65, 0.51, 0.47, 0.62, 0.50 and 0.48, respectively; the mean QR of schemes 4-9 is 0.45, 0.42, 0.34, 0.45, 0.44 and 0.33, respectively. As the spatial scale is expanded from scheme 4 to scheme 6, the calibration performance becomes worse. Schemes 7-9 give the similar

368 performance for spatial dependency. These results indicate that the gridded model
369 calibration schemes (scheme 4 and scheme 7) perform best.

370 4.3.3. Bias-corrected ET calibration versus calibration of bias-corrected PML-AET 371 combined with GRACE data

372 Both the mean NSE and mean QR of scheme 4 is relatively similar to the NSE and
373 QR in scheme 7. This is also generally true for scheme 5 versus scheme 8 and for
374 scheme 6 versus scheme 9, as show in section 4.3.2. Comparing the results of scheme
375 7 with scheme 4 in Figure 5, the mean value of NSE and QR are similar, but the range
376 of NSE becomes smaller slightly, indicated by noticeably higher NSE of daily runoff
377 at the less than 25th percentiles. This means the scheme 7 gives more stable results.
378 Similar patterns also fit at region (scheme 5 versus scheme 8) and catchment scales
379 (scheme 6 versus scheme 9). Therefore, using GRACE together with PML-AET for
380 model calibration has very limited benefit for both daily and monthly runoff
381 prediction, compared to using PML-AET solely.

382 4.3.4. RS model calibration versus traditional regionalization

383 Scheme 7 is marginally better than scheme 4, and scheme 4 is noticeably superior to
384 other PML-AET based calibration schemes. Therefore, scheme 4 is selected as the
385 best candidate to compare with scheme 2, the traditional regionalization that is
386 considered as the benchmark. In addition, the results of scheme 1, calibrated against
387 the observed runoff, are considered as the best possible result.

388 In the daily runoff simulation, schemes 1 and 2 give a mean NSE of 0.58, 0.45 and
389 mean QR of 0.33, 0.30, respectively. The mean NSE of scheme 4 decreases by 0.06
390 and mean QR of scheme 4 increases by 0.10, when compared to scheme 2. In monthly
391 runoff simulation, schemes 1 and 2 give a mean NSE of 0.72, 0.56 and mean QR of
392 0.39, 0.34, respectively. The mean NSE of scheme 4 increases by 0.09 and mean QR
393 of scheme 4 increases by 0.11, when compared with scheme 2. The mean NSE and
394 mean QR of scheme 4 are also close to those of scheme 1 especially in monthly
395 simulations. These results provide confident that model calibration against
396 bias-corrected PML-ET at each grid cell can simulate ungauged catchment and
397 regional runoff almost as well as traditional calibration and regionalization against
398 streamflow data approaches.

399 4.3.5. Summary

400 Results shown in sections 4.3.1 to 4.3.4 indicate that bias correction of PML-AET is
401 critical for improving the runoff prediction/simulation in ungauged or poorly gauged
402 catchments comparing to traditional regionalization method. The RS-based model
403 calibration framework performs better at gridded scale than at lumped scale, which
404 reflects the advantage of remote sensing in that is spatially and temporally explicit
405 across the global land surface. However, combining GRACE water storage data with
406 the bias-corrected PML-AET has very limited benefit to further improve the
407 predictions.

408 4.4. Spatial characteristics of optimum model calibration schemes

409 Figure 6 shows the NSE and QR spatial patterns from schemes 4 and 7. The NSE and
410 QR spatial patterns of schemes 4 and 7 are very similar with a difference of less than
411 0.1 in most catchments. For both schemes, the NSE of monthly runoff is generally
412 larger than the NSE of daily runoff. This is expected because of impacts of
413 precipitation seasonality (Zhang et al., 2020). Another spatial feature is that the NSE
414 values in mainstream catchments are generally larger than those in tributary
415 catchments. The NSE values of schemes 4 and 7 for Nike (05) and Lugu (24)
416 catchments are negative, but the QR values of them are positive. All in all, the NSE
417 and QR spatial patterns of schemes 4 and 7 are similar and both indicate better runoff
418 simulations in mainstream catchments than in small catchments. The result in Daluo
419 station is always good, this might be the result of the application of Q at Daluo station
420 when correcting bias of the PML-AET.

421 **Figure 6 is about here**

422 Figures 7a-7l further shows spatial patterns of performance of scheme 4 by
423 calculating the increment, compared to scheme 1 and scheme 2. Figures 7i-7l shows
424 spatial patterns of performance of scheme 7 by calculating the increment, compared to
425 scheme 4. The increments are calculated as follows:

426
$$\Delta NSE = NSE_a - NSE_b, \quad \Delta QR = QR_a - QR_b \quad (8)$$

427 where a and b refer to the proposed scheme and benchmark scheme, respectively. The
428 blue dots in Figure 7 indicate positive increments in that basin, the grey dots indicate
429 no obvious increments or decrements, and the red ones indicate negative increments.
430 The darker the color is, the greater the difference is.

431 **Figure 7 is about here**

432 Figures 7a-7d, 7e-7h, 7i-7l show the daily and monthly distribution of ΔNSE and Δ
433 QR . There are three main patterns from Figures 7a, 7e, 7i, 7c, 7g and 7k in which the
434 daily simulations are described.

435 The first pattern is that the ΔNSE of scheme 4 is greater than it of scheme 1 in 10%
436 catchments with positive ΔQR in most regions. The result shows that though scheme
437 4 performs no better than scheme 1 in most catchments but it outperforms scheme 1 in
438 certain catchment which shows the advantage of remote sensing data and gridded
439 calibration.

440 The second pattern is that in all 11 main stream stations the ΔNSE values for scheme
441 4 minus scheme 2 are positive with grey or light blue dots in daily simulations, which
442 means scheme 4 performs slightly better than scheme 2 for daily runoff simulation, in
443 upstream and large catchments which are also in main stream (e.g. Ganzi catchment).

444 Considering the model performance decided by both ΔNSE and ΔQR , scheme 4
445 performs reasonably in simulating daily runoff in downstream and small catchments,
446 compared to scheme 2.

447 The third pattern is that the combination of GRACE shows a marginal improvement
448 in most catchments according to Δ NSE, but shows slightly decrement of Δ QR in
449 downstream catchment. All in all, scheme 7 marginally improve the model
450 performance of scheme 4.

451 In monthly runoff simulation (Fig.7b, 7f, 7j, 7d, 7h, 7l), there are about 73% and 77%
452 of the catchments with no negative Δ NSE and Δ QR values for scheme 4 minus
453 scheme 1, respectively; and about 16% of catchments with negative values for both Δ
454 NSE and Δ QR for scheme 4 minus scheme 1. There are about 87% and 77% of the
455 catchments with positive Δ NSE and Δ QR values for scheme 4 minus scheme 2,
456 respectively; and only about 7% of catchments with negative values for both Δ NSE
457 and Δ QR for scheme 4 minus scheme 2. Scheme 7 performs similar to scheme 4 with
458 6% of catchments with negative values for both Δ NSE and Δ QR for scheme 7 minus
459 scheme 4.

460 In summary, in daily runoff simulations, scheme 4 performs close to scheme 1 in large
461 and main stream catchments, and outperforms scheme 1 in few catchments. Scheme 4
462 also perform better than scheme 2 in upper catchments and mainstream large
463 catchments. Scheme 4 and scheme 7 show similar performance in most regions. In
464 monthly runoff simulations, the model performance of scheme 4 against schemes 1
465 and 2 improved in upper and main stream large catchments. Scheme 4 performs no
466 worse than scheme 1 in 84% catchments and outperforms scheme 2 in 28 out of the

467 30 catchments. Overall, scheme 7 marginally improve model performance of scheme
468 4, and scheme 4 performs close to scheme 1, or better than scheme 1 in few regions.
469 scheme 4 also performs better than scheme 2 in upper catchments and mainstream
470 large catchments.

471 **5. Discussion**

472 **5.1. Potential for using RS data calibration methods**

473 The climate and topography of the Yalong River is complex and covers a wide range,
474 ranging from alpine mountains to humid basins. The complex topography and climate
475 is one of the reasons of few gauges in the Yalong River basin in its upstream alpine
476 regions. However, this region contributes majority of water resources for Jinsha River,
477 which a major tributary for the Yangtze River (Kang et al., 2001; Yang et al., 2006).
478 Therefore, it has important implication to use RS-data to calibrate hydrological
479 modelling for improving prediction skills in this region or other similar regions.

480 This study explores the performance of seven RS-data based calibration schemes in
481 30 catchments of the Yalong River basin. Though the mean NSE and QR of daily
482 runoff of schemes 4-9 are no better than that obtained from traditional regionalization
483 result (scheme 2), the performance of scheme 4 is slightly better than scheme 2 in
484 upstream and large catchments and the results of monthly runoff simulation of certain
485 schemes (schemes 4 and 7) are superior to the those obtained from scheme 2. Scheme
486 4 even outperforms scheme 1 for simulating daily runoff in a couple of catchments,

487 which demonstrates the advantage for model calibration against PML-AET at each
488 grid cell, and the advantage is more noticeable at monthly scale. This indicates that
489 the proposed approaches, especially for scheme 4, have great potential in data sparse
490 regions.

491 **5.2. Why the bias-corrected PML-AET works better**

492 Our results demonstrate that it is necessary to bias correct PML-AET data for more
493 reliable model calibration in Yalong River Basin. Since the raw PML-AET is not bias
494 corrected using water balance method, therefore, it is inevitable to get noticeable
495 biases in some areas, such as Yalong River Basin (Fig.4). The bias correction is
496 crucial in the study area as demonstrated by comparing the calibration schemes 3 and
497 4. It is noted that this study aims to improve the PML-AET model calibrations in
498 ungauged or poorly gauged catchments (Zhang et al., 2020), we use a single value of
499 mean annual runoff data in a downstream gauge and in an independent period, which
500 guarantees that the PML-AET model calibration approach having the potential for
501 large scale application. Furthermore, using a single parameter of α in Fu model can
502 generate reasonable mean annual runoff for most of the 30 catchments, demonstrating
503 that the applicability of using the downstream catchment for bias correction. All in all,
504 the bias correction method of PML-AET is reasonable with reliable gridded product
505 and limited surface data.

506 **5.3. Advantage and disadvantage of gridded model calibration**

507 Remote sensing data is gridded, and it can reduce uncertainty related to lumped
508 calibrations and gives detailed parameters for each grid (Arnold et al., 2010; Li and
509 Zhang, 2017). In this study, the gridded hydrological modelling shows great
510 advantage compared to lumped hydrological modelling. The gridded calibration
511 schemes outperform in terms of both NSE and QR compared with lumped calibration
512 schemes. It is noted that the time consumption increases by about 170 folds from
513 lumped calibration to gridded calibration. But, this cost should be paid for achieving
514 better predictions. Therefore, a more efficient algorithm is needed to reduce time
515 consumption in the future, and if necessary, a compromise should be made between
516 model accuracy and time consumption for practical application.

517 **5.4. Adding GRACE data has very limited benefit to prediction**

518 Though available studies show GRACE water storage data has been properly applied
519 in basin scales (Rodell et al., 2004), and the snow storage at high latitudes is also
520 considered in GRACE water storage data (Syed et al., 2008), this study found that the
521 benefit to include GRACE data for model calibration is limited. This could be caused
522 by the fact that the total water volume has been already properly considered by
523 bias-corrected PML-AET. Furthermore, the resolution of GRACE data is spatially (1°
524 $\times 1^\circ$) and temporally (monthly) coarse. It is probably not appropriate to apply
525 GRACE data into the small and median sized catchments located on the Yalong River

526 Basin with complex terrains and large ranges in elevations (Kang et al., 2001).
527 Therefore, more researches are needed to better utilize GRACE data for model
528 calibration in the catchments with complex terrains.

529 **5.5. Limitations and further directions**

530 This study does not consider snow cover for model calibration though the recharge
531 ratio of snowmelt runoff is relatively large, and it is the main component of runoff in
532 the upper reach of Yalong River basin (Kang et al., 2001). In addition, spring runoff
533 has a strong response to climate warming in alpine areas of Yalong River basin (Deng
534 and Hou, 1996; Liu et al., 2019a). In the future, the snow cover should be considered
535 into the upper reach catchments runoff simulation (Kang et al., 2001). However,
536 hydrological models need to be modified, making sure the modified structure has
537 physically meaningful conceptualization for appropriately assimilating remote sensing
538 data, such as snow cover and soil moisture.

539 The ‘natural flow’ is obtained by ignoring irrigation and other human-activity
540 consumption of water volume in this study. The method is reasonable during
541 2004-2012 due to less influences of reservoir dispatching. But with the running of
542 hydropower stations (such as Ertan hydropower station, Jinpin hydropower station)
543 and land use change in recent years, the human activity is severe especially in
544 downstream catchments (Liu et al., 2017; Liu et al., 2019b). For runoff simulation and
545 prediction after 2012 in Yalong River basin, a human-activity based hydrological

546 model with accurate remotely sensing data is essential and benefits both hydrology
547 and management (Montanari et al., 2013).

548 The calibration schemes still need to be improved in some aspects. Running model at
549 grids brings not only increased accuracy but also increased time consumption. In
550 addition, incorporating GRACE data improves the model stability across the selected
551 catchments though the overall improvement is marginal. Furthermore, the main
552 challenge of applying remote sensing data into rainfall-runoff modelling includes
553 choosing proper products, reducing the uncertainty of the products and matching
554 remote sensing data with model variables (Li et al., 2016). Therefore, the model
555 structure and constraining variables still need to be further developed.

556 **6. Conclusion**

557 In this study, nine modelling schemes are applied and examined for runoff prediction
558 in the Yalong River basin, an idea region for testing the benefit of using remote
559 sensing data since it has complex terrain conditions and sparse streamflow
560 observation network. The PML-AET datasets are first evaluated and then bias
561 corrected using very limited number of streamflow data. The performance of
562 calibration schemes is noticeably better after bias correction of non bias-corrected
563 PML-AET. The performance of gridded modelling is much better than lumped
564 modelling, albeit with a large increase in model run times. The calibration schemes
565 incorporating GRACE data is very limited benefit to schemes solely calibrated by

566 bias-corrected PML-AET. Using bias-corrected PML-AET to constrain gridded
567 hydrological model outperforms lumped regionalization hydrological modelling
568 (sometimes even lumped calibration against observed streamflow) especially in
569 monthly runoff simulation at upstream and large catchments. Utilizing quasi-runoff
570 free method in gridded way might improve the performance of lumped calibration
571 against observed streamflow.

572 This study implies that there is great potential to utilize and improve the runoff-free
573 (or very limited runoff) calibration method in data sparse region. In future research,
574 other remote sensing datasets (such as snow cover dataset) in both high resolution and
575 high quality should be examined to constrain model variables along with
576 incorporating human activity in ungauged catchments.

577 **Acknowledgements**

578 This study was supported by the CAS Talent Program, the National Natural Science
579 Foundation of China (Grant No. 41971032 and 51879172) and the Second Tibetan
580 Plateau Scientific Expedition and Research (2019QZKK0208). We acknowledge the
581 Yalong River hydropower development company, China, for providing daily runoff
582 data for 30 hydrology stations. PML evapotranspiration and GRACE water storage
583 data are freely available from Data Catalog of the Google Earth Engine
584 (<https://developers.google.com/earth-engine/datasets>). The Climate Meteorological
585 Forcing Dataset used in this study is provided by National Tibetan Plateau Data Center

586 (http://data.tpsc.ac.cn). Daily dataset of China's surface climate data is available from
587 the China Meteorological Data Service Center (http://data.cma.cn/). We thank
588 anonymous reviewers and editors for their critical but constructive comments on this
589 paper.

590 **Declaration of competing interest**

591 The authors declare no conflicts of interest.

592 **Author contributions**

593 YQZ conceived this study. QH prepared and performed data analysis and prepared
594 figures. QH, GHQ and YQZ wrote the paper and other authors contributed discussion
595 and interpretations of the results and manuscript revision.

596

597 **References**

- 598 Allen, R.G., Pruitt, W.O., Wright, J.L., Howell, T.A., Ventura, F., Snyder, R. , et al. (2006). A
599 recommendation on standardized surface resistance for hourly calculation of reference ETO by
600 the FAO56 Penman-Monteith method. *Agricultural Water Management*, 81(1-2), 1-22.
601 DOI:10.1016/j.agwat.2005.03.007
- 602 Arnold, J.G., Allen, P.M., Volk, M., Williams, J.R., & Bosch, D.D. (2010). Assessment of different
603 representations of spatial variability on SWAT model performance. *Transactions of the Asabe*,
604 53(5), 1433-1443.
- 605 Cheng, C., Zhao, M., Chau, K., & Wu, X. (2006). Using genetic algorithm and TOPSIS for Xinanjiang
606 model calibration with a single procedure. *Journal of Hydrology*, 316(1-4), 129-140.
- 607 Delhomme, J.P. (1978). Kriging in the Hydrosciences. *Advances in Water Resources*, 1(5), 251-266.
608 DOI:10.1016/0309-1708(78)90039-8
- 609 Deng, Y., & Hou, Y. (1996). Climatic Warming and its Impact on the Water Resources of the Yalong

610 River, China, Regional Hydrological Response to Climate Change. *Springer*, pp. 381-387.

611 Fan, Y., Lu, H., Yang, K., He, J., Wang, W., Wright Jonathon, S. , et al. (2017). Evaluation of multiple
612 forcing data sets for precipitation and shortwave radiation over major land areas of China.
613 *Hydrology & Earth System Sciences*, 21(11), 5805-5821. DOI:10.5194/hess-21-5805-2017

614 Fu, B.P. (1981). On the calculation of the evaporation from land surface. *Sci. Atmos. Sin*, 5(1), 23-31.

615 Habib, E., Haile, A.T., Sazib, N., Zhang, Y., & Rientjes, T. (2014). Effect of Bias Correction of
616 Satellite-Rainfall Estimates on Runoff Simulations at the Source of the Upper Blue Nile.
617 *Remote Sensing*, 6(7), 6688-6708. DOI:10.3390/rs6076688

618 He, J., & Yang, K. (2011). China Meteorological Forcing Dataset, Cold and Arid Regions Science Data
619 Center at Lanzhou. *Cold and Arid Regions Science Data Center at Lanzhou*.
620 DOI:10.3972/westdc.002.2014.db

621 He, J., Yang, K., Tang, W., Lu, H., Qin, J., Chen, Y. , et al. (2020). The first high-resolution
622 meteorological forcing dataset for land process studies over China. *Scientific Data*, 7(1).
623 DOI:10.1038/s41597-020-0369-y

624 Holland, J.H. (1992). Genetic Algorithms. *Scientific American*, 267(1), 66-72.
625 DOI:10.1038/scientificamerican0792-66

626 Hrachowitz, M., Savenije, H.H.G., Bloeschl, G., McDonnell, J.J., Sivapalan, M., Pomeroy, J.W. , et al.
627 (2013). A decade of Predictions in Ungauged Basins (PUB)a review. *Hydrological Sciences*
628 *Journal-Journal Des Sciences Hydrologiques*, 58(6), 1198-1255.
629 DOI:10.1080/02626667.2013.803183

630 Hundecha, Y., & Bardossy, A. (2004). Modeling of the effect of land use changes on the runoff
631 generation of a river basin through parameter regionalization of a watershed model. *Journal of*
632 *Hydrology*, 292(1-4), 281-295. DOI:10.1016/j.jhydrol.2004.01.002

633 Jayawardena, A., & Zhou, M. (2000). A modified spatial soil moisture storage capacity distribution curve
634 for the Xinanjiang model. *Journal of Hydrology*, 227(1-4), 93-113.

635 Ju, Q., Yu, Z., Hao, Z., Ou, G., Zhao, J., & Liu, D. (2009). Division-based rainfall-runoff simulations
636 with BP neural networks and Xinanjiang model. *Neurocomputing*, 72(13-15), 2873-2883.

637 Kang, E., Cheng, G., Lan, Y., & Chen, X. (2001). Alpine runoff simulation of the Yalong River for the
638 south-north water diversion. *J Glaciol Geocryol*, 23(1), 139-148.

639 Konak, A., Coit, D.W., & Smith, A.E. (2006). Multi-objective optimization using genetic algorithms: A
640 tutorial. *Reliability Engineering & System Safety*, 91(9), 992-1007.
641 DOI:10.1016/j.ress.2005.11.018

642 Kundu, D., Vervoort, R.W., & van Ogtrop, F.F. (2017). The value of remotely sensed surface soil
643 moisture for model calibration using SWAT. *Hydrological Processes*, 31(15), 2764-2780.
644 DOI:10.1002/hyp.11219

645 Landerer, F.W., & Swenson, S. (2012). Accuracy of scaled GRACE terrestrial water storage estimates.
646 *Water resources research*, 48(4).

647 Li, H., & Zhang, Y. (2017). Regionalising rainfall-runoff modelling for predicting daily runoff:
648 Comparing gridded spatial proximity and gridded integrated similarity approaches against their
649 lumped counterparts. *Journal of Hydrology*, 550, 279-293. DOI:10.1016/j.jhydrol.2017.05.015

650 Li, H., Zhang, Y., Chiew, F.H., & Xu, S. (2009). Predicting runoff in ungauged catchments by using
651 Xinanjiang model with MODIS leaf area index. *Journal of Hydrology*, 370(1-4), 155-162.

652 Li, Y., Grimaldi, S., Walker, J.P., & Pauwels, V.R.N. (2016). Application of Remote Sensing Data to
653 Constrain Operational Rainfall-Driven Flood Forecasting: A Review. *Remote Sensing*, 8(6).
654 DOI:10.3390/rs8060456

655 Liu, X., Chen, R., Liu, J., Wang, X., Zhang, B., Han, C., et al. (2019a). Effects of snow-depth change on
656 spring runoff in cryosphere areas of China. *Hydrological Sciences Journal*, 64(7), 789-797.

657 Liu, X., Peng, D., & Xu, Z. (2017). Identification of the impacts of climate changes and human activities
658 on runoff in the Jinsha River Basin, China. *Advances in Meteorology*, 2017.

659 Liu, X., Yang, M., Meng, X., Wen, F., & Sun, G. (2019b). Assessing the impact of reservoir parameters
660 on runoff in the Yalong River Basin using the SWAT Model. *Water*, 11(4), 643.

661 Merz, R., & Blöschl, G. (2004). Regionalisation of catchment model parameters. *Journal of Hydrology*,
662 287(1-4), 95-123. DOI:10.1016/j.jhydrol.2003.09.028

663 Montanari, A., Young, G., H, H.G.S., D, H., T, W., L, L., Ren, et al. (2013). “Panta Rhei—Everything
664 Flows”: Change in hydrology and society—The IAHS Scientific Decade 2013–2022.
665 *Hydrological Sciences Journal*, 58(6), 1256-1275. DOI:10.1080/02626667.2013.809088

666 Nash, J.E., & Sutcliffe, J.V. (1970). River flow forecasting through conceptual models part I — A
667 discussion of principles. *Journal of Hydrology*, 10(3), 282-290.
668 DOI:https://doi.org/10.1016/0022-1694(70)90255-6

669 Oudin, L., Andreassian, V., Perrin, C., Michel, C., & Le Moine, N. (2008). Spatial proximity, physical
670 similarity, regression and ungauged catchments: A comparison of regionalization approaches
671 based on 913 French catchments. *Water Resources Research*, 44(3).
672 DOI:10.1029/2007wr006240

673 Pechlivanidis, I.G., & Arheimer, B. (2015). Large-scale hydrological modelling by using modified PUB
674 recommendations: the India-HYPE case. *Hydrology and Earth System Sciences*, 19(11),
675 4559-4579. DOI:10.5194/hess-19-4559-2015

676 Pomeon, T., Diekkruuger, B., Springer, A., Kusche, J., & Eicker, A. (2018). Multi-Objective Validation
677 of SWAT for Sparsely-Gauged West African River Basins-A Remote Sensing Approach. *Water*,
678 10(4). DOI:10.3390/w10040451

679 Post, D.A., & Jakeman, A.J. (1999). Predicting the daily streamflow of ungauged catchments in SE

680 Australia by regionalising the parameters of a lumped conceptual rainfall-runoff model.
681 *Ecological Modelling*, 123(2-3), 91-104. DOI:10.1016/s0304-3800(99)00125-8

682 Ren, M., Xu, Z., Pang, B., Liu, W., & Liu, J. (2018). Accuracy Evaluation of A Variety of
683 Satellite-Derived Precipitation Products in Beijing City. *AGUFM*, 2018, H33I-2211.

684 Rodell, M., Famiglietti, J.S., Chen, J., Seneviratne, S.I., Viterbo, P., Holl, S. , et al. (2004). Basin scale
685 estimates of evapotranspiration using GRACE and other observations. *Geophysical Research*
686 *Letters*, 31(20). DOI:10.1029/2004gl020873

687 Standardization Administration of the People's Republic of China, & General Administration of Quality
688 Supervision, Inspection and Quarantine of the People's Republic of China. (2008).Standard for
689 Hydrological Information And Hydrological forecasting. Standards Press of China.

690 Stisen, S., & Sandholt, I. (2010). Evaluation of remote-sensing-based rainfall products through
691 predictive capability in hydrological runoff modelling. *Hydrological Processes*, 24(7), 879-891.
692 DOI:10.1002/hyp.7529

693 Sutanudjaja, E.H., van Beek, L.P.H., de Jong, S.M., van Geer, F.C., & Bierkens, M.F.P. (2014).
694 Calibrating a large-extent high-resolution coupled groundwater-land surface model using soil
695 moisture and discharge data. *Water Resources Research*, 50(1), 687-705.
696 DOI:10.1002/2013wr013807

697 Swenson, S., & Wahr, J. (2006). Post-processing removal of correlated errors in GRACE data.
698 *Geophysical Research Letters*, 33(8).

699 Syed, T.H., Famiglietti, J.S., Rodell, M., Chen, J., & Wilson, C.R. (2008). Analysis of terrestrial water
700 storage changes from GRACE and GLDAS. *Water Resources Research*, 44(2).
701 DOI:10.1029/2006wr005779

702 Wanders, N., Bierkens, M.F.P., de Jong, S.M., de Roo, A., & Karssenber, D. (2014). The benefits of
703 using remotely sensed soil moisture in parameter identification of large-scale hydrological
704 models. *Water Resources Research*, 50(8), 6874-6891. DOI:10.1002/2013wr014639

705 Wu, Y., Guo, L., Zheng, H., Zhang, B., & Li, M. (2019). Hydroclimate assessment of gridded
706 precipitation products for the Tibetan Plateau. *Science of The Total Environment*, 660,
707 1555-1564.

708 Yadav, M., Wagener, T., & Gupta, H. (2007). Regionalization of constraints on expected watershed
709 response behavior for improved predictions in ungauged basins. *Advances in Water Resources*,
710 30(8), 1756-1774. DOI:10.1016/j.advwatres.2007.01.005

711 Yang, F., Lu, H., Yang, K., Wang, W., Li, C., Han, M. , et al. (2017). Evaluation and comparison among
712 multiple forcing data sets for precipitation and shortwave radiation over mainland China.
713 *Hydrology and Earth System Sciences Discussions*, 21(11), 1-32.

714 Yang, Z., Wang, H., Saito, Y., Milliman, J.D., Xu, K., Qiao, S. , et al. (2006). Dam impacts on the

715 Changjiang (Yangtze) River sediment discharge to the sea: The past 55 years and after the Three
716 Gorges Dam. *Water Resources Research*, 42(4). DOI:10.1029/2005wr003970

717 Yao, C., Li, Z., Bao, H., & Yu, Z. (2009). Application of a developed Grid-Xinjiang model to Chinese
718 watersheds for flood forecasting purpose. *Journal of Hydrologic Engineering*, 14(9), 923-934.

719 Yassin, F., Razavi, S., Wheeler, H., Sapriza-Azuri, G., Davison, B., & Pietroniro, A. (2017). Enhanced
720 identification of a hydrologic model using streamflow and satellite water storage data: A
721 multicriteria sensitivity analysis and optimization approach. *Hydrological Processes*, 31(19),
722 3320-3333. DOI:10.1002/hyp.11267

723 Zhang, L., Hickel, K., Dawes, W., Chiew, F.H., Western, A., & Briggs, P. (2004). A rational function
724 approach for estimating mean annual evapotranspiration. *Water resources research*, 40(2).

725 Zhang, L., Potter, N., Hickel, K., Zhang, Y., & Shao, Q. (2008). Water balance modeling over variable
726 time scales based on the Budyko framework—Model development and testing. *Journal of*
727 *Hydrology*, 360(1-4), 117-131.

728 Zhang, X., & Tang, Q. (2015). Combining satellite precipitation and long-term ground observations for
729 hydrological monitoring in China. *Journal of Geophysical Research-Atmospheres*, 120(13),
730 6426-6443. DOI:10.1002/2015jd023400

731 Zhang, Y., & Chiew, F.H.S. (2009). Relative merits of different methods for runoff predictions in
732 ungauged catchments. *Water Resources Research*, 45(7). DOI:10.1029/2008wr007504

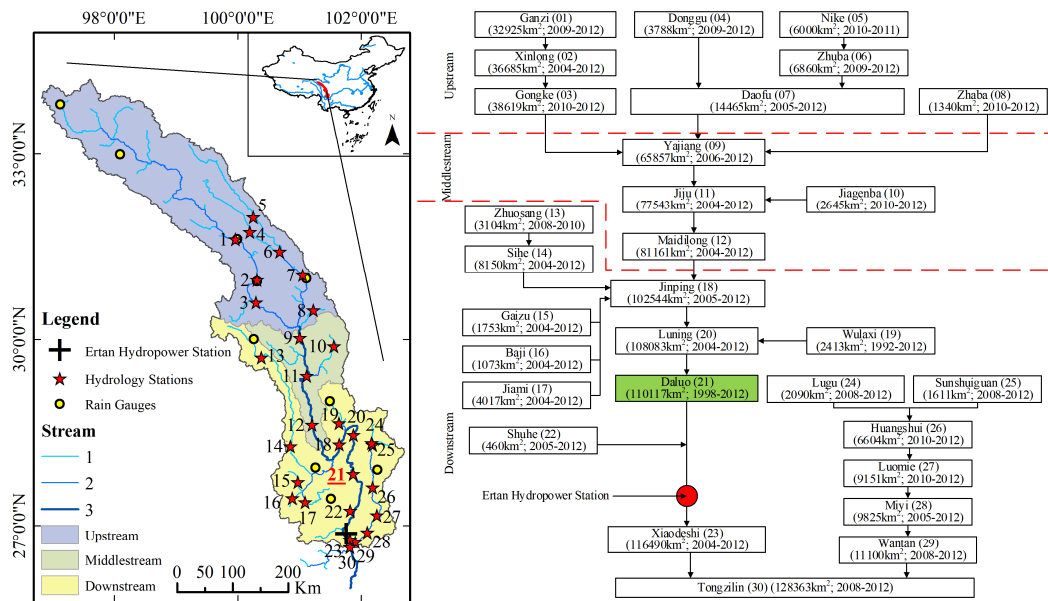
733 Zhang, Y., Chiew, F.H.S., Liu, C., Tang, Q., Xia, J., Tian, J., et al. (2020). Can Remotely Sensed Actual
734 Evapotranspiration Facilitate Hydrological Prediction in Ungauged Regions Without Runoff
735 Calibration? *Water Resources Research*, 56(1). DOI:10.1029/2019wr026236

736 Zhang, Y., Kong, D., Gan, R., Chiew, F.H.S., McVicar, T.R., Zhang, Q., et al. (2019). Coupled estimation
737 of 500 m and 8-day resolution global evapotranspiration and gross primary production in 2002–
738 2017. *Remote Sensing of Environment*, 222, 165-182.
739 DOI:https://doi.org/10.1016/j.rse.2018.12.031

740 Zhao, R.J. (1980). The xinjiang model, Proceedings of the Oxford Symposium.

741 Zhao, R.J. (1992). The Xinjiang model applied in China. *Journal of Hydrology*, 135(1-4), 371-381.

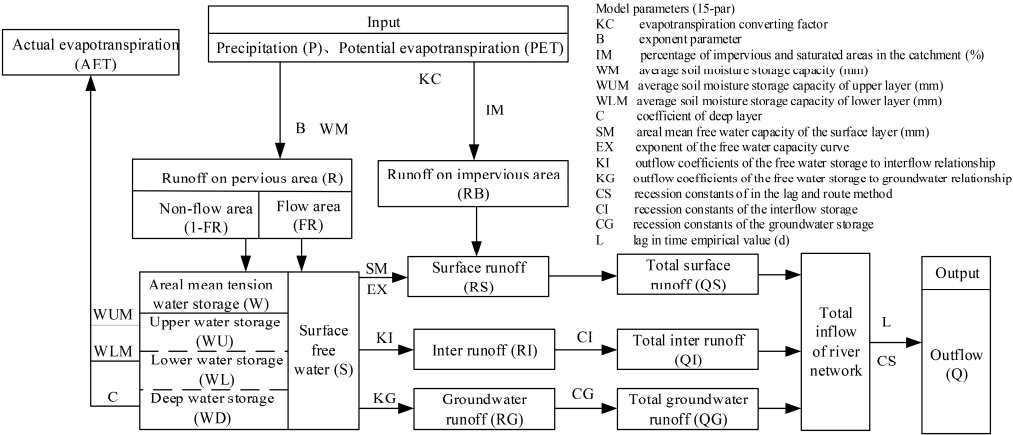
742 **Figures and figure captions**



744 **Figure 1.** Information and location of study area. The station Daluo for constraining

745 Fu model is labelled as 21.

746



747 **Figure 2.** Model structure of Xinanjiang Model

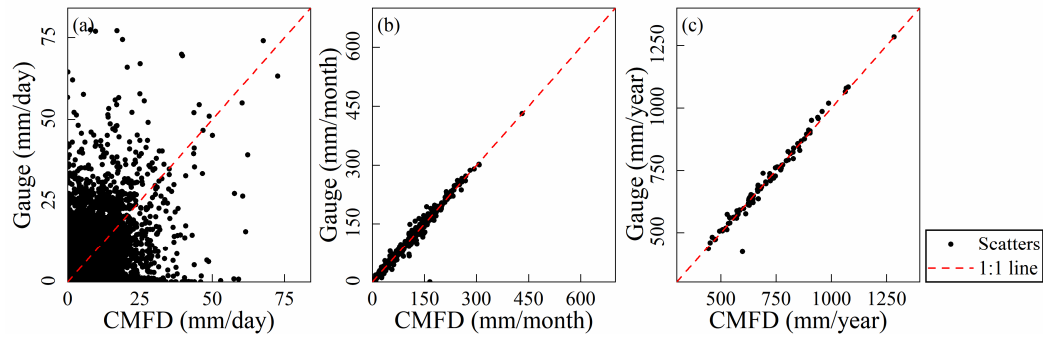
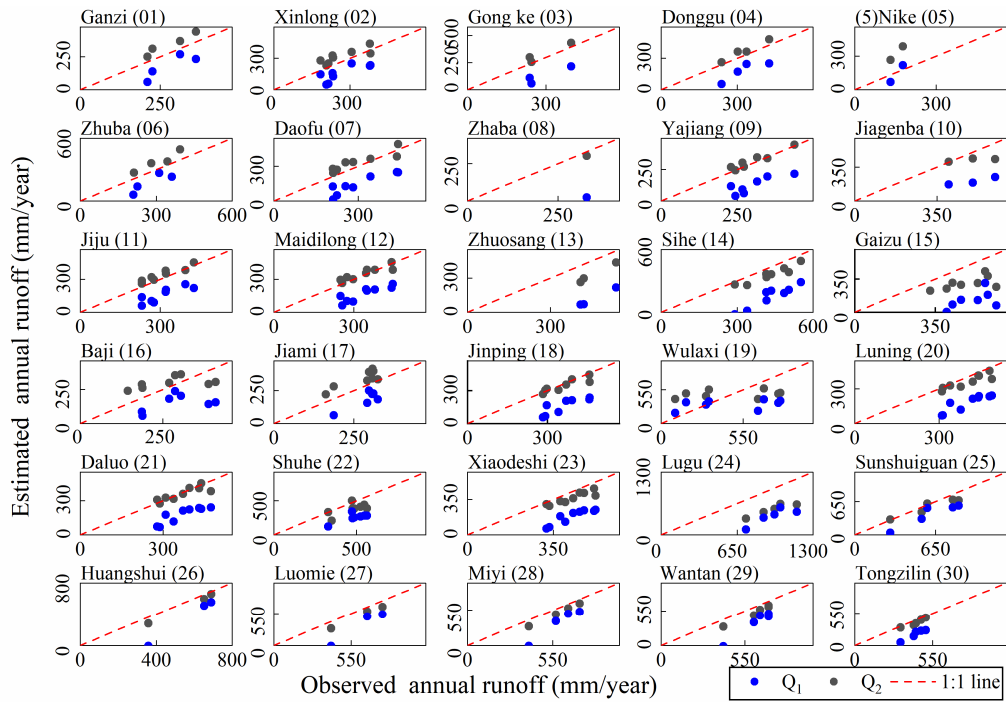


Figure 3. Comparison between observed precipitation and precipitation generated from CMFD data (CMFD-P)



751

752

Figure 4. Evaluating annual runoff obtained from precipitation minus non

753

bias-corrected PML-AET (Q_1) and that (Q_2) obtained from precipitation minus bias

754

corrected PML-AET (The numbers in the bracket represent the watershed codes shown

755

in Figure 1.)

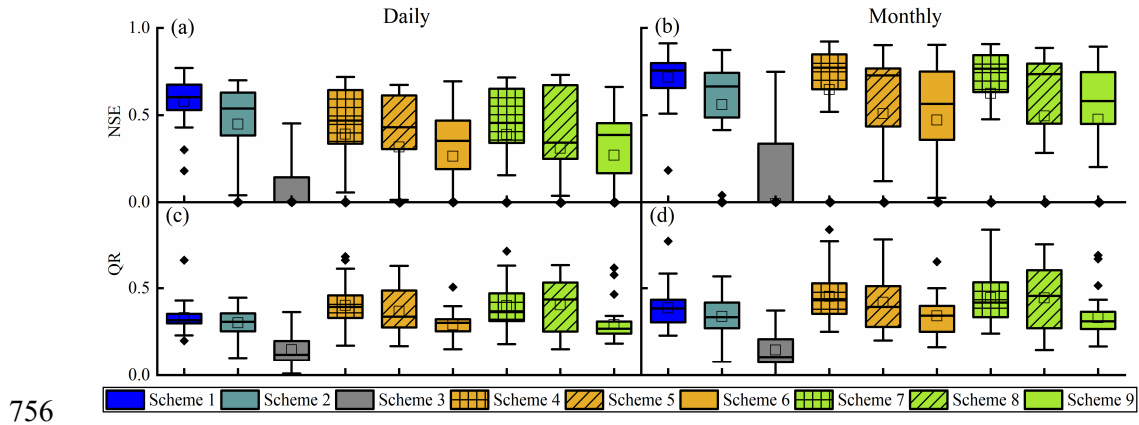
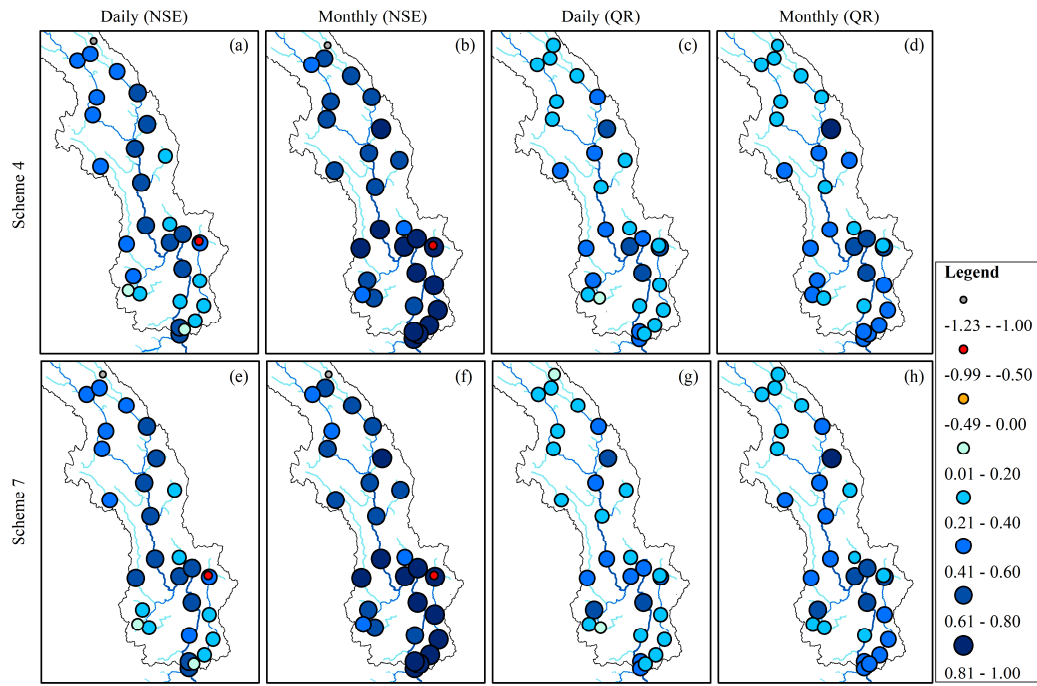


Figure 5. Comparison of performance of the nine calibration schemes for estimating streamflow. Noted that negative NSE values are plotted as zero for better visualization (The boxes represent the values range from 25th to 75th percentiles, the lines in each plot from top to bottom represent upper boundary, median value and lower boundary, respectively. The square represents the mean value and the rhombus represents the outlier.)



763

764 **Figure 6.** NSE and QR spatial patterns obtained from scheme 4 and scheme 7

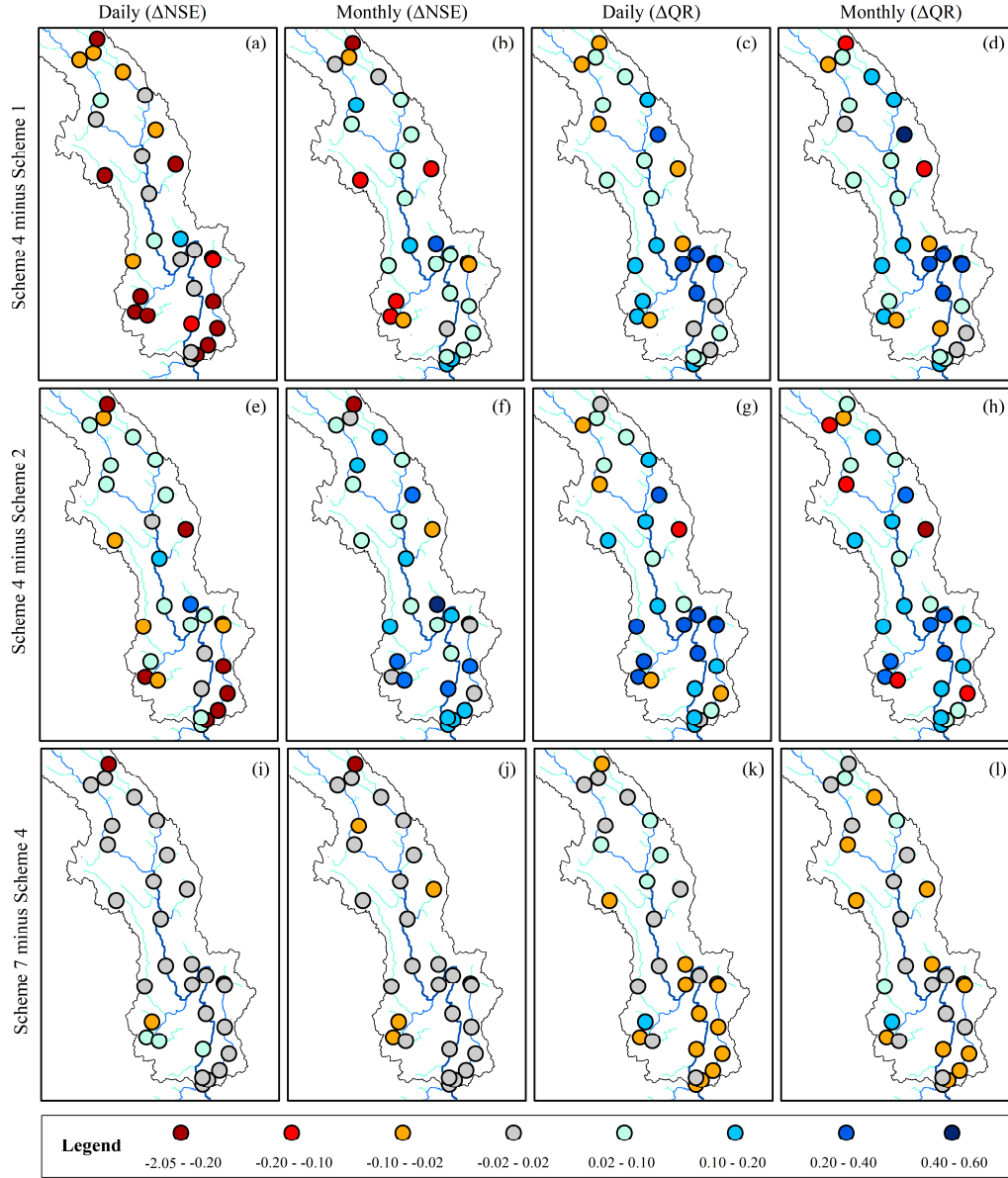


Figure 7. Spatial evaluation of scheme 4 against scheme 1, 2 and 7. The difference among them is obtained from Equation (8). Having a range from -0.02 to 0.02, gray means the two perform similarly.